Subkelvin Parametric Feedback Cooling of a Laser-Trapped Nanoparticle

Jan Gieseler,[1] Bradley Deutsch,[3] Romain Quidant,[1,2] and Lukas Novotny[3,4]

[1]*ICFO-Institut de Ciencies Fotoniques, Mediterranean Technology Park, 08860 Castelldefels (Barcelona), Spain*
[2]*ICREA-Institució Catalana de Recerca i Estudis Avançats, 08010 Barcelona, Spain*
[3]*Institute of Optics, University of Rochester, Rochester, New York 14627, USA*
[4]*Photonics Laboratory, ETH Zürich, 8093 Zürich, Switzerland*

(Received 6 June 2012; published 7 September 2012)

We optically trap a single nanoparticle in high vacuum and cool its three spatial degrees of freedom by means of active parametric feedback. Using a *single* laser beam for both trapping and cooling we demonstrate a temperature compression ratio of four orders of magnitude. The absence of a clamping mechanism provides robust decoupling from the heat bath and eliminates the requirement of cryogenic precooling. The small size and mass of the nanoparticle yield high resonance frequencies and high quality factors along with low recoil heating, which are essential conditions for ground state cooling and for low decoherence. The trapping and cooling scheme presented here opens new routes for testing quantum mechanics with mesoscopic objects and for ultrasensitive metrology and sensing.

DOI: 10.1103/PhysRevLett.109.103603 PACS numbers: 42.50.Wk, 07.10.Pz, 62.25.Fg

The interaction between light and matter sets ultimate limits on the accuracy of optical measurements. Braginsky predicted that the finite response time of light in an optical interferometer can lead to mechanical instabilities [1] and impose limits on the precision of laser-based gravitational interferometers. Later, it was demonstrated that this "dynamic back-action mechanism" can be used to reduce the oscillation amplitude of a mechanical system and to effectively cool it below the temperature of the environment [2–7] and even to its quantum ground state [8–10]. In addition to the fascinating possibility of observing the quantum behavior of a mesoscopic system, many applications have been proposed for such systems ranging from detection of exotic forces [11–13] to the generation of nonclassical states of light and matter [14,15].

Most of the mechanical systems studied previously are directly connected to their thermal environment, which imposes limits to thermalization and decoherence. As a consequence, clamped systems require cryogenic precooling. A laser-trapped particle in ultrahigh vacuum, by contrast, has no physical contact to the environment [16,17], which makes it a promising system for ground state cooling even at room temperatures [14,15]. Cooling of micron-sized particles to millikelvin temperatures has recently been achieved by applying an *active* optical feedback inspired by atom cooling experiments [18]. A particle is trapped by two counter-propagating beams and cooling is performed with three additional laser beams via radiation pressure. However, because light scattering leads to recoil heating there is a limit for the lowest attainable temperature. Eliminating recoil heating as the limiting factor for ground state cooling requires considerably smaller mechanical systems, such as single dielectric nanoparticles [14,15]. Here we demonstrate optical trapping in high vacuum of a fused silica nanoparticle of radius $R \sim 70$ nm. Additionally, we employ a novel cooling scheme based on the optical gradient force to cool its motional degrees of freedom from room temperature to $\sim$50 mK (compression factor of $\sim 10^4$).

In our experiments we use a laser beam of wavelength $\lambda = 1064$ nm (~ 100 mW), focused by a lens with numerical aperture 0.8 mounted in a vacuum chamber. A single nanoparticle is trapped by means of the optical gradient force, which points towards the center of the trap for all translational degrees of freedom of the nanoparticle (c.f. Fig. 1). For particles much smaller than the wavelength, the polarizability scales as $\alpha \propto R^3$ and the

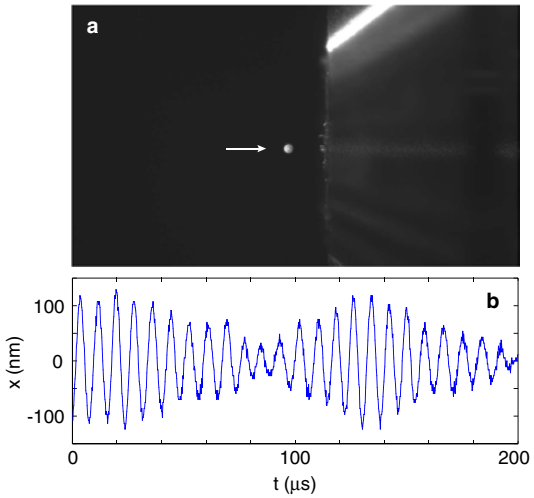

FIG. 1 (color online). Trapping of a nanoparticle. (a) Photograph of light scattered from a trapped silica nanoparticle (arrow). The object to the right is the outline of the objective that focuses the trapping laser. (b) Time trace of the particle's x coordinate (transverse to the optical axis) at 2 mbar pressure.

gradient force dominates over the scattering force. Scattered light from the particle is measured interferometrically with three separate photodetectors that render the particle's motion in the x, y, and z directions [19]. This phase-sensitive detection scheme makes use of balanced detection and yields a noise floor of $\sim 1.2\ \mathrm{pm}/\sqrt{\mathrm{Hz}}$. Figure 1 shows a photograph of a trapped nanoparticle along with a typical time trace of the particle's x coordinate. Trapping times of more than 60 h have been achieved at pressures below 10^{-5} mbar indicating that the particle's internal temperature does not affect the center-of-mass motion [14] and that melting of the particle is not a concern.

To control and stabilize the particle's motion in the optical trap we implemented an active feedback loop. All three spatial degrees of freedom are controlled with the same laser used for trapping. To cool the center-of-mass motion of the particle we employ a *parametric* feedback scheme, similar to parametric amplification of laser fields [20] and stabilization of nanomechanical oscillators [21]. After trapping a single nanoparticle at ambient temperature and pressure we evacuate the vacuum chamber in order to reach the desired vacuum level. At ambient pressure the particle's motion is dominated by the viscous force (Stokes force) due to the random impact of gas molecules. However, as shown in Fig. 1(b), the inertial force dominates in a vacuum of a few millibars as the particle's motion becomes ballistic [22].

Parametric feedback is activated as soon as we enter the ballistic regime. In a time-domain picture, the feedback loop hinders the particle's motion by increasing the trap stiffness whenever the particle moves away from the trap center and reducing it when the particle falls back toward the trap. In the frequency domain, this corresponds to a modulation at twice the trap frequency with an appropriate phase shift. Our parametric feedback is fundamentally different from previous active feedback schemes based on radiation pressure [23]. Radiation pressure acts only along the direction of beam propagation and therefore requires a separate cooling laser for every oscillation direction [18]. In contrast, the gradient force points towards the center of the trap, thus allowing us to cool all three directions with a single laser beam.

Figure 2 illustrates our parametric feedback mechanism. To obtain a signal at twice the oscillation frequency we multiply the particle's position $x(t)$ with it's time derivative. The resulting signal $x(t)\dot{x}(t)$ is then phase-shifted by a controlled amount in order to counteract the particle's oscillation. Note that depending on the latency of the feedback loop, we can achieve damping or amplification of the particle's oscillation. In the absence of active feedback, the particle's oscillation naturally locks to the modulation phase in such a way as to achieve amplification [20]. Cooling therefore requires active feedback to adjust the modulation phase constantly.

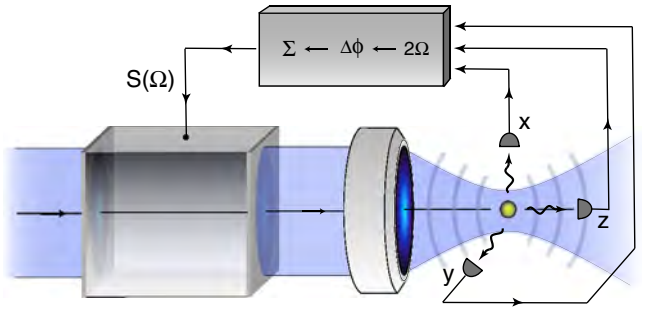

FIG. 2 (color online). Principle of parametric feedback cooling. The center-of-mass motion of a laser-trapped nanoparticle in ultrahigh vacuum is measured interferometrically with three detectors, labeled x, y, and z. Each detector signal is frequency doubled and phase shifted. The sum of these signals is used to modulate the intensity of the trapping beam.

In our cooling scheme, frequency doubling and phase shifting is done independently for each of the photodetector signals x, y, and z. Since the three directions are spectrally separated [see Fig. 3(b)], there is no cross-coupling between the three signals, that is, modulating one of the signals does not affect the other signals. Therefore, it is possible to sum up all three feedback signals and use the result to drive a single Pockels cell that modulates the power P of the trapping laser. Thus, using a single beam we are able to effectively cool all spatial degrees of freedom.

For small oscillation amplitudes, the trapping potential is harmonic and the three spatial dimensions are decoupled. Each direction can be characterized by a frequency Ω_0, which is defined by the particle mass m and

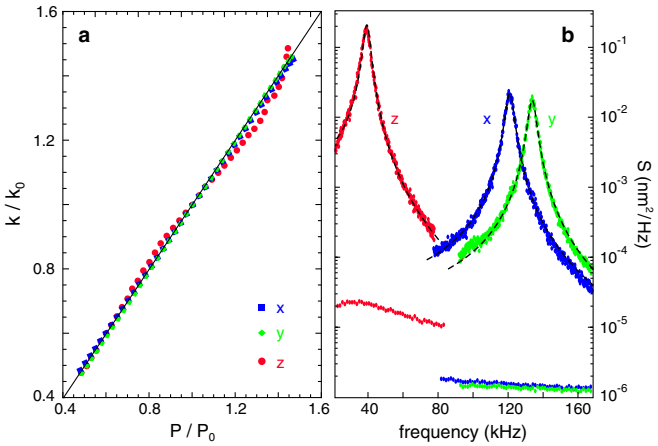

FIG. 3 (color online). Trap stiffness and spectral densities. (a) Normalized trap stiffness in the x, y, and z directions as a function of normalized laser power. Dots are experimental data and the solid line is a linear fit. (b) Spectral densities of the x, y, and z motions. The trapped particle has a radius of $R = 69$ nm and the pressure is $P_{\mathrm{gas}} = 6.3$ mbar. The resonance frequencies are $f_0 = 37$ kHz, 120 kHz, and 134 kHz, respectively. The dashed curves are fits according Eq. (4) and the data on the bottom correspond to the noise floor.

the trap stiffness k_{trap} as $\Omega_0 = \sqrt{k_{\mathrm{trap}}/m}$. The equation of motion for the particle's motion in x direction (polarization direction) is

$$\ddot{x}(t) + \Gamma_0 \dot{x}(t) + \Omega_0^2 x(t) = \frac{1}{m}[F_{\mathrm{fluct}}(t) + F_{\mathrm{opt}}(t)], \quad (1)$$

where F_{fluct} is a random Langevin force that satisfies $\langle F_{\mathrm{fluct}}(t) F_{\mathrm{fluct}}(t')\rangle = 2m\Gamma_0 k_B T \delta(t - t')$ according to the fluctuation-dissipation theorem. $F_{\mathrm{opt}}(t) = \Delta k_{\mathrm{trap}}(t)\, x(t)$ is a time-varying, nonconservative optical force introduced by parametric feedback. It leads to shifts $\delta\Gamma$ and $\delta\Omega$ in the particle's natural damping rate Γ_0 and oscillation frequency Ω_0, respectively. Similar equations and considerations hold for the particle's motion in y and z directions.

We first consider the particle's dynamics with the feedback loop deactivated. For small oscillation amplitudes, the particle experiences a harmonic trapping potential with a trap stiffness k_{trap}, which is a linear function of P. In the paraxial and dipole approximations (small particle limit, weak focusing) the *transverse* trap stiffness is calculated as [19]

$$k_{\mathrm{trap}} = 4\pi^3 \frac{\alpha P}{c\varepsilon_0} \frac{(\mathrm{NA})^4}{\lambda^4}, \quad (2)$$

where ε_0 is the vacuum permittivity, NA is the numerical aperture of the focused beam, λ is the wavelength, and α is the particle polarizability. A similar expression holds for the *longitudinal* trap stiffness. For the parameters used in our experiments we find that the particle's oscillation frequency in x direction is $f_0^{(x)} = (k_{\mathrm{trap}}/m)^{1/2}/(2\pi) = 120$ kHz. For the axial oscillation frequency we find $f_0^{(z)} = 37$ kHz and for the y direction we measure $f_0^{(y)} = 134$ kHz. The different oscillation frequencies in x and y directions originate from the symmetry of the laser focus [24]. The linear dependence of the trap stiffness on laser power has been verified for all three directions and is shown in Fig. 3(a). In Fig. 3(b) we show the spectral densities of the x, y, and z motions recorded at a pressure of $P_{\mathrm{gas}} = 6.3$ mbar.

Once a particle has been trapped, the interaction with the background gas thermalizes its energy with the environment and, according to the fluctuation-dissipation theorem, damps the particle's motion with the rate Γ_0 in Eq. (1). From kinetic theory we find that [18,25]

$$\Gamma_0 = \frac{6\pi\eta R}{m} \frac{0.619}{0.619 + \mathrm{Kn}}(1 + c_K), \quad (3)$$

where $c_K = 0.31\ \mathrm{Kn}/(0.785 + 1.152\ \mathrm{Kn} + \mathrm{Kn}^2)$, η is the viscosity coefficient of air and $\mathrm{Kn} = \bar{l}/R$ is the Knudsen number. When the mean free path $\bar{l} \propto 1/P_{\mathrm{gas}}$ is much larger than the radius of the particle, Γ_0 becomes proportional to P_{gas}. Figure 4 shows the measured value of Γ_0 for all three directions as a function of pressure. For a pressure of $P_{\mathrm{gas}} = 10^{-5}$ mbar we measure a damping of $\Gamma_0/2\pi = 10$ mHz,

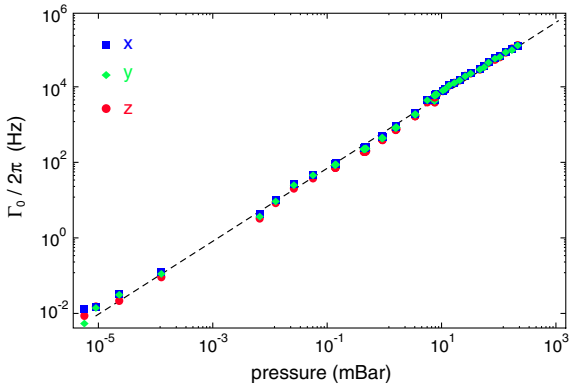

FIG. 4 (color online). Damping rate as a function of gas pressure. The damping rate Γ_0 decreases linearly with pressure P_{gas}. The dashed line is a fit according to Eq. (3).

which corresponds to a quality factor of $Q = 10^7$, a value that is higher than the quality factors achieved with clamped oscillators [26]. In ultrahigh vacuum ($P_{\mathrm{gas}} = 10^{-9}$ mbar), the quality factor will reach values as high as $Q \sim 10^{11}$.

Activation of the parametric feedback loop gives rise to additional damping $\delta\Gamma$ and a frequency shift $\delta\Omega$. The resulting spectral line shapes are defined by the power spectral density $S_x(\Omega)$, which follows from Eq. (1) as

$$S_x(\Omega) = \int_{-\infty}^{\infty} \langle x(t)x(t - t')\rangle e^{-i\Omega t'} dt' = \frac{\Gamma_0 k_B T/(\pi m)}{([\Omega_0 + \delta\Omega]^2 - \Omega^2)^2 + \Omega^2[\Gamma_0 + \delta\Gamma]^2}. \quad (4)$$

Integrating both sides over Ω yields the mean square displacement

$$\langle x^2\rangle = \langle x(0)x(0)\rangle = \frac{k_B T}{m(\Omega_0 + \delta\Omega)^2} \frac{\Gamma_0}{\Gamma_0 + \delta\Gamma}. \quad (5)$$

According to the equipartition principle, the center-of-mass temperature $T_{\mathrm{c.m.}}$ follows from $k_B T_{\mathrm{c.m.}} = m(\Omega_0 + \delta\Omega)^2\langle x^2\rangle$. Considering that $\delta\Omega \ll \Omega_0$ we obtain

$$T_{\mathrm{c.m.}} = T \frac{\Gamma_0}{\Gamma_0 + \delta\Gamma}, \quad (6)$$

where T is the equilibrium temperature in the absence of the parametric feedback ($\delta\Gamma = 0$). Thus, the temperature of the oscillator can be raised or lowered, depending on the sign of $\delta\Gamma$ in Eq. (6).

The experimental results of parametric feedback cooling are shown in Fig. 5, which depicts the dependence of the center-of-mass temperature $T_{\mathrm{c.m.}}$ on pressure. The cooling action of the feedback loop competes with reheating due to collisions with air molecules, ultimately setting a minimum achievable temperature for each pressure value. Since the area under the line shape defined in Eq. (4) is proportional to $T_{\mathrm{c.m.}}$, feedback cooling not only increases the linewidth but also lowers the signal amplitude until it

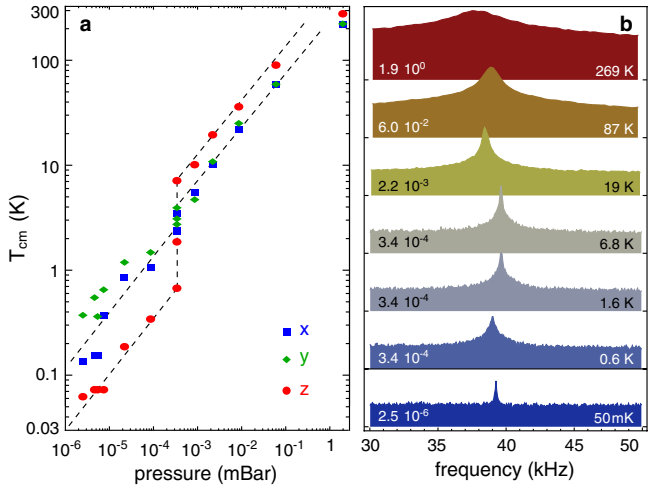

FIG. 5 (color online). Parametric feedback cooling. (a) Dependence of the center-of-mass temperature $T_{\mathrm{c.m.}}$ on pressure. The cooling rate (the slope of the dashed lines) is similar for the different directions x, y, and z. The feedback gain has been increased at a pressure of ~ 0.3 μBar causing a kink in the curves. (b) Spectra of the z motion evaluated for different pressures and temperatures $T_{\mathrm{c.m.}}$. The area under the curves is proportional to $T_{\mathrm{c.m.}}$. The numbers in the figure indicate the pressure in mbar.

reaches the noise floor. Nevertheless, we are able to reach temperatures of $T_{\mathrm{c.m.}} \sim 50$ mK while maintaining the particle in the trap.

In the quantum limit, a mechanical oscillator exhibits discrete states separated in energy by $\hbar(\Omega_0 + \delta\Omega) \sim \hbar\Omega_0$. The mean thermal occupancy is

$$\langle n \rangle = \frac{k_B T_{\mathrm{c.m.}}}{\hbar\Omega_0}. \tag{7}$$

In order to resolve the quantum ground state we require $\langle n \rangle < 1$. For a 120 kHz oscillator, this condition implies $T_{\mathrm{c.m.}} \sim 6$ μK. According to Eq. (6), a low pressure implies a low damping rate and thus, extrapolating Fig. 5(a), we find that this temperature will be reached at ultrahigh vacuum (10^{-11} mbar), provided that the particle oscillation can be measured and the feedback remains operational. Alternatively, lower occupancy can be reached at higher pressures by an increase of the feedback gain. Laser power noise introduces fluctuations in the trap stiffness and therefore in the mechanical oscillation frequency. We believe that the resulting random phase error in the feedback loop is the current limiting factor in cooling. This phase error can be minimized by using background suppression and laser stabilization techniques [27]. The noise floor in our measurements is currently 1.2 pm/$\sqrt{\mathrm{Hz}}$.

In feedback cooling, the particle's position has to be measured in order to operate the feedback loop. Measurement uncertainty of x, y, and z introduced by shot noise therefore limits the lowest attainable temperature $T_{\mathrm{c.m.}}$. The measurement accuracy is fundamentally limited by the standard quantum limit [19], which follows from the uncertainty principle $\Delta x \Delta p \geq \hbar/2$, where $\Delta p = \Delta n \hbar k$, Δn being the uncertainty in photon number and $k = 2\pi/\lambda$. For shot noise $\Delta n \propto N^{1/2}$, where N is the mean photon number $N = P\Delta t/(\hbar k c)$. In terms of the bandwidth $B = 1/\Delta t$ we obtain $\Delta x \geq [\hbar c \lambda B/(8\pi P)]^{1/2}$. Thus, the measurement uncertainty is determined by the bandwidth B and the signal power P at the detector. For a $R \sim 70$ nm nanoparticle and the parameters used in our experiments we find $\Delta x \geq 6.3$ pm, which corresponds to a center-of-mass temperature of $T_{\mathrm{c.m.}} = 5.6$ μK [19]. Thus, in absence of backaction, parametric feedback should allow us to cool a laser-trapped nanoparticle close to its quantum ground state.

Evidently, the measurement uncertainty Δx can be reduced by increasing the signal power at the detector, for example by higher laser power or by using a larger particle size R and, hence, a larger scattering cross section $\sigma_{\mathrm{scatt}} = k^4 |\alpha|^2/(6\pi\varepsilon_0^2)$. However, strong scattering introduces recoil heating, which destroys the coherent particle motion [19]. In analogy to atomic trapping, the transition rate Γ_{recoil} between consecutive harmonic oscillator states is calculated as [14,19]

$$\Gamma_{\mathrm{recoil}} = \frac{2}{5}\left[\frac{\hbar k^2/2m}{\Omega_0}\right]\left[\frac{I_0 \sigma_{\mathrm{scatt}}}{\hbar\omega}\right], \tag{8}$$

where I_o is the laser intensity at the focus. The last term in brackets corresponds to the photon scattering rate. Comparing Γ_{recoil} with the frequency of a center-of-mass oscillation Ω_0 we find that in the current configuration there is only one recoil event per ~ 10 oscillations. Thus, the trapped nanoparticle can coherently evolve for many oscillation periods. The number of coherent oscillations in between recoil events N_{osc} scales with the ratio $(\lambda/R)^3$, so small particles and long wavelengths are favorable.

Our discussion highlights the tradeoff between measurement uncertainty and recoil heating. A nanoparticle of size of $R \sim 70$ nm is a good compromise between the two limiting factors. Notice that Γ_{recoil} and the photon scattering rate differ by a factor of $\sim 10^{-9}$, and hence most of the scattered photons do not alter the center-of-mass state of the particle. The possibility of observing the particle without destroying its quantum coherence is a critical advantage over atomic trapping and cooling experiments. Finally, parametric cooling should work even without continuously tracking $x(t)$ as long as the frequency and the phase of the center-of-mass oscillation are known.

In conclusion, we have demonstrated that an optically trapped nanoparticle in high vacuum can be efficiently cooled in all three dimensions by a parametric feedback scheme. The parametric feedback makes use of a *single* laser beam and is therefore not limited by alignment inaccuracies of additional cooling lasers. Theoretical considerations show that center-of-mass temperatures close to the quantum ground state are within reach. To fully exploit the quantum coherence of a laser-trapped nanoparticle,

parametric feedback cooling can be combined with *passive* dynamical back-action cooling [28], for example, by use of optical cavities [10,14] or electronic resonators [9]. The results shown here also hold promise for ultrasensitive detection and sensing [11]. The ultrahigh quality factors and small oscillation amplitudes yield force sensitivities on the order of 10^{-20} N/$\sqrt{\text{Hz}}$ [29], which outperforms most other ultrasensitive force measurement techniques by orders of magnitude, and can find applications for the detection of single electron or nuclear spins [30], Casimir forces and vacuum friction, phase transitions, and non-Newtonian gravitylike forces [11].

This research was funded by the U.S. Department of Energy (Grant No. DE-FG02-01ER15204), Fundació Privada CELLEX, and ERC-Plasmolight (No. 259196). We thank Mathieu Juan and Vijay Jain for valuable input and help.

[1] V. B. Braginsky, *Measurement of Weak Forces in Physics Experiments* (University of Chicago, Chicago, 1977).
[2] C. Höhberger Metzger and K. Karrai, Nature (London) **432**, 1002 (2004).
[3] P. F. Cohadon, A. Heidmann, and M. Pinard, Phys. Rev. Lett. **83**, 3174 (1999).
[4] O. Arcizet, P. F. Cohadon, T. Briant, M. Pinard, and A. Heidman, Nature (London) **444**, 71 (2006).
[5] S. Gigan, H. R. Bohm, M. Paternostro, F. Blaser, G. Langer, J. B. Hertzberg, K. C. Schwab, D. Bauerle, M. Aspelmeyer, and A. Zeilinger, Nature (London) **444**, 67 (2006).
[6] A. Schliesser, P. Del'Haye, N. Nooshi, K. J. Vahala, and T. J. Kippenberg, Phys. Rev. Lett. **97**, 243905 (2006).
[7] K. Usami, A. Naesby, T. Bagci, B. M. Nielsen, J. Liu, S. Stobbe, P. Lodahl, and E. S. Polzik, Nature Phys. **8**, 168 (2012).
[8] J. Chan, T. P. M. Alegre, A. H. Safavi-Naeini, J. T. Hill, A. Krause, S. Gröblacher, M. Aspelmeyer, and O. Painter, Nature (London) **478**, 89 (2011).
[9] J. D. Teufel, T. Donner, D. Li, J. W. Harlow, M. S. Allman, K. Cicak, A. J. Sirois, J. D. Whittaker, K. W. Lehnert, and R. W. Simmonds, Nature (London) **475**, 359 (2011).
[10] E. Verhagen, S. Deléglise, S. Weis, A. Schliesser, and T. J. Kippenberg, Nature (London) **482**, 63 (2012).
[11] A. A. Geraci, S. B. Papp, and J. Kitching, Phys. Rev. Lett. **105**, 101101 (2010).
[12] O. Romero-Isart, A. C. Pflanzer, M. L. Juan, R. Quidant, N. Kiesel, M. Aspelmeyer, and J. I. Cirac, Phys. Rev. A **83**, 013803 (2011).
[13] A. Manjavacas and F. J. García de Abajo, Phys. Rev. Lett. **105**, 113601 (2010).
[14] D. E. Chang, C. A. Regal, S. B. Papp, D. J. Wilson, J. Ye, O. Painter, H. J. Kimble, and P. Zoller, Proc. Natl. Acad. Sci. U.S.A. **107**, 1005 (2009).
[15] O. Romero-Isart, M. L. Juan, R. Quidant, and J. I. Cirac, New J. Phys. **12**, 033015 (2010).
[16] A. Ashkin and J. M. Dziedzic, Appl. Phys. Lett. **28**, 333 (1976).
[17] A. Ashkin and J. M. Dziedzic, Appl. Phys. Lett. **30**, 202 (1977).
[18] T. Li, S. Kheifets, and M. G. Raizen, Nature Phys. **7**, 527 (2011).
[19] See Supplemental Material at http://link.aps.org/supplemental/10.1103/PhysRevLett.109.103603 for experimental setup, measurement procedures, derivation of trap stiffness, and limits of measurement accuracy.
[20] A. Yariv, *Quantum Electronics* (Wiley, New York, 1989), 3rd ed..
[21] L. G. Villanueva, R. B. Karabalin, M. H. Matheny, E. Kenig, M. C. Cross, and M. L. Roukes, Nano Lett. **11**, 5054 (2011).
[22] T. Li, S. Kheifets, D. Medellin, and M. Raizen, Science **328**, 1673 (2010).
[23] M. Poggio, C. L. Degen, H. J. Mamin, and D. Rugar, Phys. Rev. Lett. **99**, 017201 (2007).
[24] L. Novotny and B. Hecht, *Principles of Nano-Optics* (Cambridge University Press, Cambridge, England, 2006).
[25] S. A. Beresnev, V. G. Chernyak, and G. A. Fomyagin, J. Fluid Mech. **219**, 405 (1990).
[26] M. Poot and H. S. J. van der Zant, Phys. Rep. **511**, 273 (2012).
[27] F. Seifert, P. Kwee, M. Heurs, B. Willke, and K. Danzmann, Opt. Lett. **31**, 2000 (2006).
[28] T. J. Kippenberg and K. J. Vahala, Opt. Express **15**, 17172 (2007).
[29] B. C. Stipe, H. J. Mamin, T. D. Stowe, T. W. Kenny, and D. Rugar, Phys. Rev. Lett. **86**, 2874 (2001).
[30] D. Rugar, R. Budakian, H. Mamin, and B. Chui, Nature (London) **430**, 329 (2004).

Supplementary Information

Sub-Kelvin Parametric Feedback Cooling of a Laser-Trapped Nanoparticle

Jan Gieseler[1], Bradley Deutsch[3], Romain Quidant[1,2] and Lukas Novotny[3]

1. ICFO-Institut de Ciencies Fotoniques, Mediterranean Technology Park, 08860 Castelldefels (Barcelona), Spain.
2. ICREA-Institució Catalana de Recerca i Estudis Avançats, 08010 Barcelona, Spain.
3. Institute of Optics, University of Rochester, Rochester, NY 14627, USA.

1 Experimental setup

Light from the laser source is separated into two orthogonal polarizations. One polarization is frequency shifted by an acousto-optic modulator to avoid interference due to polarization mixing in the laser focus (Fig. S1a). Before entering the chamber the two orthogonally polarized beams are recombined and focused by a high NA objective to form the single beam trap.

The motion of the particle $x(t)$ is imprinted on the phase of the scattered light $E_s \propto \exp ikx(t)$. This light interferes with the non-scattered light which propagates in the same direction. As a result, the phase modulation is transduced into an intensity modulation. The total light intensity is collimated by an aspheric lens (Fig. S1b) and sent to three photodetectors. Splitting part of the collimated beam vertically and part of it horizontally, we produce signals that are proportional to particle displacements in the x and y directions, respectively (see Section 2) [1]. A signal proportional to the displacement in z direction is obtained by balanced detection, where one of the light beams is the detection beam and the other a constant reference (Fig. S1c). After the chamber, a combination of a $\lambda/2$-waveplate and polarizing beamsplitter is used to separate the two polarizations. This results in two beams of different polarizations, one of which is not affected by modulation of the Pockels cell and is used for detection. The three electronic signals from the balanced photodetectors are send to the electronic feedback loop

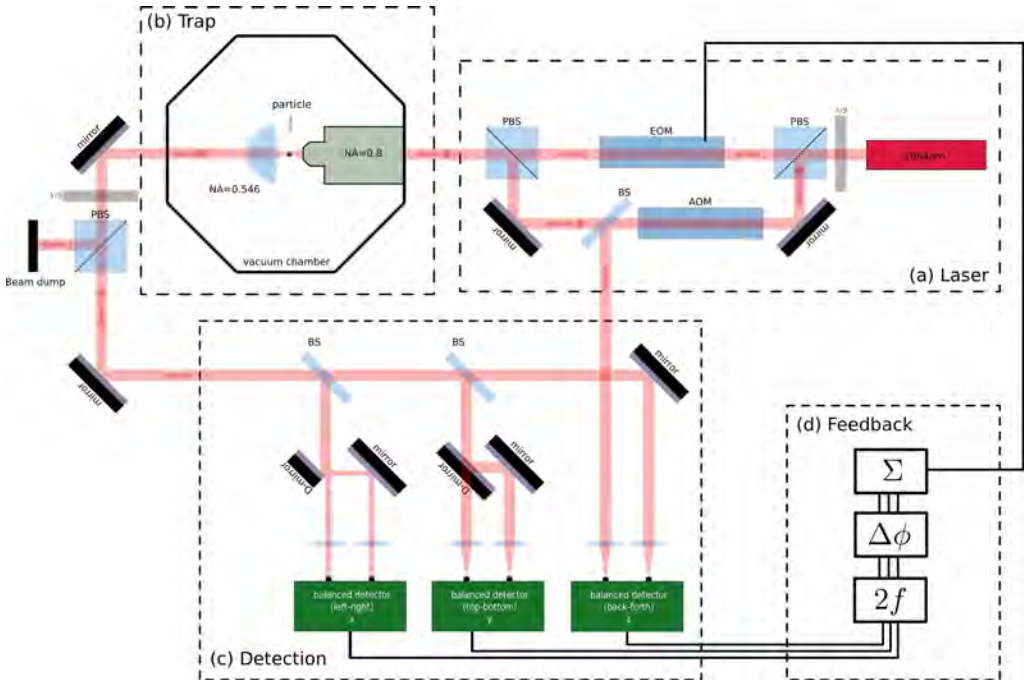

Figure S1: *a) The laser light is split into two orthogonally polarized beams. One is frequency shifted by an acousto-optic modulator and serves as a probe beam. The other is modulated by an electro-optic modulator and traps and cools the particle. b.) The parts of the beam are re-combined and focused by a microscope objective. After the vacuum chamber the polarizations are separated. c.) To detect all three directions of motion, we use three balanced detectors. d.) The detector signals are frequency doubled, then phase shifted and finally added together to generate the feedback signal that drives the Pockels cell.*

which produces the feedback signal as explained in the main text. This signal is then sent to the Pockels cell which modulates the intensity of the trapping laser (Fig. S1d).

[1] Gittes, F. & Schmidt, C. F. Interference model for back-focal-plane displacement detection in optical tweezers. *Optics letters* **23**, 7–9 (1998).

2 Detector signal

To analyze the detector signal, we consider an incident Gaussian beam polarized along x

$$\mathbf{E}_{00}(\mathbf{r}) = E_0 \frac{w_0}{w(z)} e^{-\frac{\rho^2}{w(z)^2}} e^{i\left(kz - \eta(z) + \frac{k\rho^2}{2R(z)}\right)} \mathbf{n}_x \tag{1}$$

with beam waist $w(z) = w_0\sqrt{1 + z^2/z_0^2}$, wavefront radius $R(z) = z\left(1 + z_0^2/z^2\right)$ and phase correction $\eta(z) = \text{acrtan}\left(z/z_0\right)$. The incident field excites a dipole moment $\mu_{\text{dp}}\left(\mathbf{r}_{\text{dp}}\right) = \alpha\, \mathbf{E}_{00}\left(\mathbf{r}_{\text{dp}}\right)$ in the particle

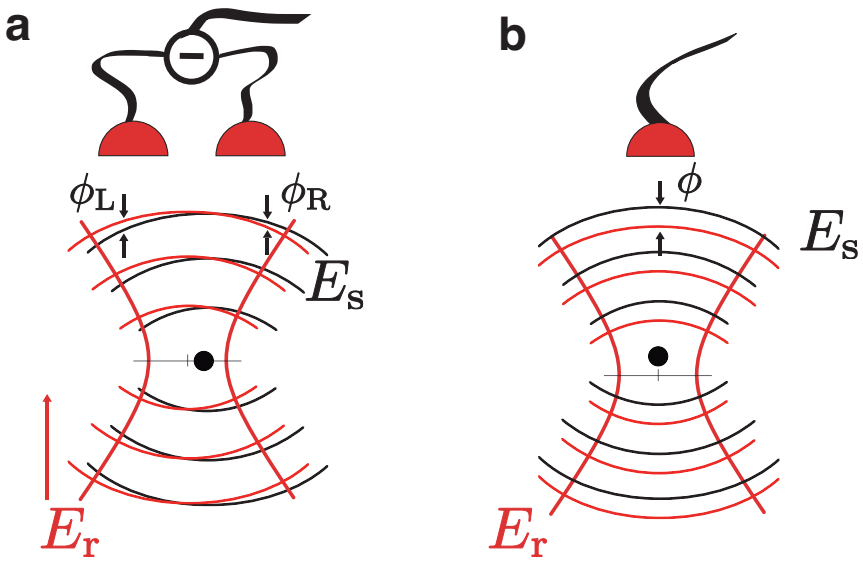

Figure S2: **Optical detection of the particle position.** *a) To detect lateral displacements, the transmitted light is split and the two resulting beams are detected in differential mode. Because scattered light from the particle travels distances that are different for the two detectors, the accumulated phase at each detector is different. At the detector the scattered light interferes with the unscattered light, which serves as reference beam, making the detector signal sensitive to changes in the phase. Since the phase depends on the position of the particle, the detector signal is proportional to the motion of the particle. b.) To detect the motion along the optical axis, the entire transmitted beam is detected. The total intensity at the detector is the sum of scattered light and unscattered light. The latter serves as a reference, whereas the former has a phase that depends on the particle's position on the optical axis. Due to interference of the two, the detector signal is sensitive to the phase and therefore to the position of the particle. Note that this detection is not dependent on lateral displacement as the phase due to lateral displacements at one half of the detector cancels with the phase at the other half of the detector.*

situated at $\mathbf{r}_{dp}$ with polarizability $\alpha = 4\pi\epsilon_0 a^3(\epsilon_p - 1)/(\epsilon_p + 2)$, dielectric constant ϵ_p and radius a. The induced dipole in turn radiates an electric field

$$\mathbf{E}_{\text{Dipole}}(\mathbf{r}, \mathbf{r}_{\text{dp}}) = \omega^2 \mu_0 \mathbf{G}(\mathbf{r}, \mathbf{r}_{\text{dp}}) \mu_{\text{dp}}, \tag{2}$$

where $\mathbf{G}(\mathbf{r}, \mathbf{r}_{\text{dp}})$ is the dyadic Green's function [1] of an electric dipole loacted at $\mathbf{r}_{\text{dp}}$. Applying the paraxial approximation ($z \ll x, y$, hence $z \approx r$), we can write the respective far fields of the unscattered and scattered fields at the as

$$\mathbf{E}_{00}^{ff}(\mathbf{r}) = E_{\text{ref}} \exp i(kR - \pi/2)\mathbf{n}_x \tag{3}$$

and

$$\mathbf{E}_{\text{Dipole}}^{ff}(\mathbf{r}, \mathbf{r}_{\text{dp}}) = E_{\text{dp}} \exp i(kR + \phi_{\text{dp}})\mathbf{n}_x, \tag{4}$$

where $E_{\text{dp}} = E_0 \alpha \omega^2 \mu_0 / 4\pi R \, \exp(-\rho_{\text{dp}}^2 / w_0^2)$ and $E_{\text{ref}} \approx E_0 z_0 / R \, \exp(-\rho^2 / w_\infty^2)$ are the amplitudes of the fields at the detector located at a distance R from the focus. The transmitted light beam undergoes a phase shift of $\pi/2$, know as the Guoy phase shift. The phase $\phi_{\text{dp}} = -\mathbf{k} \cdot \mathbf{r}_{\text{dp}} + \left(k - \frac{1}{z_0}\right) z_{\text{dp}}$ of the scattered field is modulated by the motion $\mathbf{r}_{\text{dp}}(t)$ of the particle.

At the detector, the fields interfere and produce an intensity distribution proportional to

$$I(\mathbf{r}, \mathbf{r}_{\text{dp}}) \propto |\mathbf{E}_{\text{total}}|^2 = \left|\mathbf{E}_{\text{dp}} + \mathbf{E}_{\text{ref}}\right|^2 = E_{\text{dp}}^2 + 2E_{\text{dp}} E_{\text{ref}} \sin\left(\phi_{\text{dp}}(\mathbf{r}, \mathbf{r}_{\text{dp}})\right) + E_{\text{ref}}^2. \tag{5}$$

The first term of the last expression in (5) is small compared to the other two and can be neglected. The collector lens images the momentum distribution with $\mathbf{k} = \mathbf{x}k/R$. Integrating (5) over the detector area, the dependency on x and y vanishes due to the symmetry and the detector output only depends on z. For small displacements z_{dp} we can expand the $\sin$ in (5) and get a signal $\propto E_{\text{dp}} E_{\text{ref}} \, z_{\text{dp}}/z_0$ plus a constant term $\propto E_{\text{ref}}^2$. For the detection of the lateral displacements x and y, we split the beam vertically and horizontally, respectively. The two resulting beams are detected with a balanced detector. Due to the balanced detection, the constant term in (5) as well as the dependency on z and on the orthogonal displacement cancels and we measure a signal $\propto E_{\text{dp}} E_{\text{ref}} \, x_{\text{dp}}/w_0$ for x and the corresponding signal for y.

[1] Novotny, L. & Hecht, B. *Principles of Nano-Optics* (Cambridge University Press, Cambridge, 2006).

3 Derivation of the trap stiffness

For a dipolar particle, the gradient force in a monochromatic field $\mathbf{E}$ is given by [1]

$$\mathbf{F} \;=\; \frac{\alpha}{4}\,\nabla\left[\mathbf{E}\cdot\mathbf{E}^{*}\right]\;, \tag{6}$$

where $\alpha = 4\pi\varepsilon_0 R^3[\varepsilon-1]/[\varepsilon+2]$ is the polarizability of a particle with radius R and dielectric constant ε. For a Gaussian laser beam we find

$$\nabla\left[\mathbf{E}\cdot\mathbf{E}^{*}\right]|_{y,z=0} \;=\; -E_0^2\,[4x/w_0^2] \tag{7}$$

$$\nabla\left[\mathbf{E}\cdot\mathbf{E}^{*}\right]|_{x,y=0} \;=\; -E_0^2\,[4z/w_0^2]\,[2/(kw_0)^2] \tag{8}$$

where we have expanded in a series around the focal point and kept only the lowest-order (linear) terms. w_0 is the beam waist radius and $k = 2\pi/\lambda$. Defining the trap stiffnesses as

$$\mathrm{F_x} \;=\; -\,k_{\mathrm{trap}}^{(x)}\,x\,, \quad \mathrm{F_z} \;=\; -\,k_{\mathrm{trap}}^{(z)}\,z\,, \tag{9}$$

expressing the field in the focus by the incident power as $P = (\pi/4)\;E_0^2\;w_0^2\;\varepsilon_0\,c$, and using $w_0 = \lambda/(\pi\,\mathrm{NA})$ (paraxial approximation) yields

$$k_{\mathrm{trap}}^{(x)} \;=\; \frac{4\alpha\,\mathrm{NA}^4\pi^3}{c\epsilon_0\lambda^4}P\,, \quad k_{\mathrm{trap}}^{(z)} \;=\; \frac{2\alpha\,\mathrm{NA}^6\pi^3}{c\epsilon_0\lambda^4}P\,. \tag{10}$$

[1] Novotny, L. & Hecht, B. *Principles of Nano-Optics* (Cambridge University Press, Cambridge, 2006).

4 Limits of the measurement accuracy

In this section, we show that measurement backaction ultimately limits the accuracy with which a particle can be measured. To accurately measure the particle's position, we need to minimize shot noise due to the discrete nature of photons. This can only be accomplished by using a large number of photons and hence a high laser power. On the other hand, high laser power gives rise to large radiation pressure, which leads to a perturbation of the particle's position.

4.1 The standard quantum limit

Photons that scatter off the particle carry information about the particle's position. A photodetector records the scattered photons and yields a signal that is proportional to the particle's position. The

stochastic arrival of photons adds an uncertainty to the measurement. For scattered light composed of N photons, the uncertainty in photon number is $\Delta n = \sqrt{N}$ (shot noise), which yields a momentum uncertainty of

$$\Delta p = \sqrt{N}\hbar k\,. \tag{11}$$

where $k = \omega/c$ is the photon wavenumber. According to the uncertainty principle, the minimum position uncertainty follows from $\Delta x \Delta p = \hbar/2$, that is,

$$\Delta x = \frac{1}{2k\sqrt{N}}\,. \tag{12}$$

Thus, a position measurement improves as the number of photons N is increased. On the other hand, large photon numbers lead to a large momentum spread and hence to an increased probability to excite transitions between the states of the mechanical oscillator, which are separated in energy by $\hbar\Omega_0$.

The fluctuations of the oscillator's energy (noise) depends both on Δx and Δp and is calculated as

$$\Delta U = \frac{1}{2}\left(m\Omega_0^2\Delta x^2 + \frac{\Delta p^2}{m}\right)\,. \tag{13}$$

The first part is the measurement uncertainty due to the random arrival of photons and the second part is the measurement backaction due to momentum transfer. The lowest noise, known as the standard

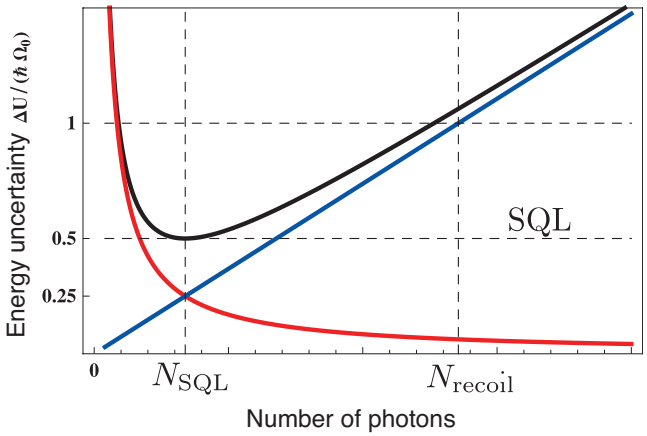

Figure S3: **The standard quantum limit.** *The standard quantum limit is reached when the measured position uncertainty of the particle equals the momentum uncertainty due to photon recoil. The horizontal axis denotes the number of scattered photons N within the measurement time. The red curve shows the measurement uncertainty, the blue curve the measurement backaction, and the black curve is the sum of the two.*

quantum limit (SQL), is found when the measurement back-action equals the measurement imprecision (c.f. Fig. S3). Inserting Eqs. (11) and (12) yields a minimum for $N = N_{\mathrm{SQL}} = m\Omega_0/(2\hbar k^2)$.

4.2 Recoil heating

The recoil imparted on the particle by a scattered photon is a small effect since the photon momentum is small compared to the momentum of the mechanical oscillator. However, at very low temperatures and pressures, collisions with air molecules become negligible and photon recoil takes over as the dominating decoherence process.

The number of photons N_{recoil} required to excite a transition between the oscillator's states follows from the energy balance

$$N_{\mathrm{recoil}} \frac{\hbar^2 k^2}{2m} \;=\; \hbar\Omega_0 \,, \tag{14}$$

where $\hbar^2 k^2/2m$ is the recoil energy of a single photon and $\hbar\Omega_0$ is the energy separation between oscillator states. Thus, at least $N_{\mathrm{recoil}} = 2m\Omega_0/(\hbar k^2)$ photons need to interact with the oscillator to add one quantum of mechanical energy. Note that N_{recoil} is differs by a factor of 4 from N_{SQL} derived previously (c.f. Fig. S3).

The particle's efficiency to scatter light is represented by the scattering cross section $\sigma_{\mathrm{scat}} = k^4|\alpha|^2/(6\pi\varepsilon_o^2)$, where α is the particle's polarizability. The number of photons scattered in a time interval Δt follows from $N_{\mathrm{scat}} = P_{\mathrm{scat}}\,\Delta t/(\hbar\omega)$, P_{scat} being the scattered power. In terms of the scattering cross section, P_{scat} can be expressed as $P_{\mathrm{scat}} = \sigma_{\mathrm{scat}} I_0$. Here, $I_0 = P_0/\sigma_{\mathrm{focus}}$ is the intensity at the laser focus, P_0 the incident power, and σ_{focus} the focal area of the laser beam.

The time Δt that it takes to acquire $N_{\mathrm{scat}} = N_{\mathrm{recoil}}$ photons and hence to excite a transition between oscillator states can be calculated by combining the different equations. The recoil rate is the inverse of this time and becomes

$$\Gamma_{\mathrm{recoil}} = \frac{1}{\Delta t_{\mathrm{recoil}}} = \left[\frac{\hbar^2 k^2/2m}{\hbar\Omega_0}\right]\left[\frac{I_0\,\sigma_{\mathrm{scatt}}}{\hbar\omega}\right] \,. \tag{15}$$

A more detailed calculation, taking the dipole radiation pattern of the particle into account, yields a factor of $2/5$ (see main text) [1].

4.3 Detection bandwidth

Experimentally, the measurement time Δt is defined by the detection bandwidth $B \approx 1/\Delta t$. Using $N_{\text{scat}} = P_{\text{scat}}\Delta t/(\hbar\omega)$ we find that the position uncertainty Δx defined in Eq. (12) is

$$\Delta x = \sqrt{\frac{\hbar c \lambda B}{8\pi P_{\text{scat}}}}. \tag{16}$$

For the parameters used in our experiments ($R = 70\,$nm, $P_0 = 100\,$mW, $\lambda = 1064\,$nm and $B = 300\,$kHz) we find $N_{\text{scat}} \approx 10^8$ and a position uncertainty of $\Delta x \approx 6.3\,$pm, which is of the order of the zero point motion (see main text). Our experimental parameters are therefore close to the optimum.

Eq. (16) predicts that the position accuracy can be improved by reducing the detection bandwidth B. However, for the feedback to work we need to be be able to resolve the particle's amplitude $A(t)$ and phase $\phi(t)$.[1] The classical trajectory of the particle can be represented as $x(t) = A(t)\sin(\Omega_0 t + \phi(t))$, where $A(t)$ and $\phi(t)$ are slowly varying functions that vary over timescales Δt_{meas} much larger than the time defined by our detection bandwidth. In other words, the maximum measurement time Δt_{meas} that is available for the measurement of $x(t)$ is the time over which $x(t+\Delta t_{\text{meas}})$ remains correlated with $x(t)$.

In ultrahigh vacuum, the dominant decoherence process is recoil heating and therefore $\Delta t_{\text{meas}} = 1/\Gamma_{\text{recoil}}$, which depends on the scattered power P_{scat}. Using $B \approx \Gamma_{\text{recoil}}$ in Eq. (16), the position accuracy becomes independent of power. This is a direct manifestation of the uncertainty principle, which states that the minimum uncertainty corresponds to the zero point motion.

Ultimately, one is interested in the number of coherent oscillations N_{osc} that can be observed. Employing the expression for the trap stiffness derived in section 3, we find that the number

$$N_{\text{osc}} = \frac{\Omega_0}{2\pi\Gamma_{\text{recoil}}} \propto \frac{1}{(kR)^3}\,, \tag{17}$$

which doesn't depend on power either. Hence, we can choose a laser power that is sufficiently high to make photon shot noise the dominant noise source and to make electronic noise (detector dark current, Johnson noise) irrelevant. Note that N_{osc} strongly depends on the particle size, which is the primary motivation for using nanoscale particles as opposed to microspheres.

In conclusion, we have shown that neither the number of coherent oscillations, nor the minimum position uncertainty depend on power. As a consequence, we can work in a regime where the measurement uncertainty is only limited by photon shot noise. In that case, the minimum measurement uncertainty is achieved by a detection bandwidth of $B \approx \Gamma_{\text{recoil}}$.

[1] In principle, only the phase is needed for the feedback to work. The amplitude is required for reading out the particle's energy and temperature.

[1] D. E. Chang, C. A. Regal, S. B. Papp, D. J. Wilson, J. Ye, O. Painter, H. J. Kimble, and P. Zoller, "Cavity opto-mechanics using an optically levitated nanosphere," Proceedings of the National Academy of Sciences **107**, 1005–1010 (2010).

5 Backaction with active feedback

Besides the measurement backaction derived in the previous section, there is also noise introduced by the feedback loop, which tends to heat the oscillator. To understand how measurement imprecision affects the performance of the feedback, we consider the mean energy of the harmonic oscillator

$$U = \frac{\hbar\Omega_0}{2}\left[\langle\delta p\rangle^2 + \langle\delta x\rangle^2\right] = \hbar\Omega_0\left(n_{\text{eff}} + \frac{1}{2}\right), \tag{18}$$

where the two oscillator variances are given by integrating the corresponding fluctuation spectrum

$$\langle\delta x\rangle^2 = \int_{-\infty}^{\infty}\frac{d\Omega}{2\pi}S_x(\Omega) \quad \langle\delta p\rangle^2 = \int_{-\infty}^{\infty}\frac{d\Omega}{2\pi}\frac{\Omega^2}{\Omega_0^2}S_x(\Omega)\ . \tag{19}$$

According to linear feedback theory [1], the position spectrum with parametric feedback can be expressed as[2]

$$S_x(\Omega) = |\chi_{\text{eff}}(\Omega)|^2\left[S_{\text{th}}(\Omega) + S_{\text{opt}}(2\Omega) + S_{\text{fb}}(2\Omega)\right], \tag{20}$$

where χ_{eff} is the effective susceptibility of the oscillator, modified by the feedback, S_{th} is the thermal noise spectrum, S_{opt} is the noise spectrum of the light field and S_{fb} is the noise contribution due to the measurement noise, that is fed back into the oscillator by the feedback loop. Due to parametric coupling of the optical gradient force to the oscillator, the position spectrum depends on the second harmonic of the feedback and optical noise spectrum.

From (20) it becomes clear that the feedback contributes twofold to the position spectrum. On the one hand it attenuates the particle's susceptibility χ_{eff}, and on the other hand it introduces a noise term S_{fb} due to measurement imprecision of the particle's position. For low gain, the thermal noise spectrum dominates over the feedback noise spectrum and the position spectrum is reduced due to the modified susceptibility. For large gain, however, the feedback noise dominates the thermal noise

[2]The effective susceptibility is given by $|\chi_{eff}(\Omega)|^2 = \frac{1/4\pi m^2}{([\Omega_0+\delta\Omega]^2-\Omega^2)^2+\Omega^2[\Gamma_0+\delta\Gamma]^2}$ and the thermal force noise by $S_{\text{th}} = \frac{4m\Omega_0}{Q}\frac{1}{2}\hbar\Omega\coth\left(\hbar\Omega/2k_BT\right)$. In the limit $k_BT \gg \hbar\Omega$, $S_{\text{th}} = 4mk_BT\Omega_0$ and we recover equation (4) from the main text.

and the the position spectrum increases. The optimum gain is found when thermal noise and feedback noise contribute equally to the position uncertainty. To minimize the noise contribution of the feedback the position measurement should be shot noise limited.

In section 2 we showed that the interferometric signal is $S \propto E_r E_s x$. The noise due to the random arrival of photons at the detector is $\propto \sqrt{P} \propto \sqrt{|E_r|^2}$. The signal-to-noise ratio, therefore, depends on the magnitude of the scattered light and the displacement x but not on the magnitude of the reference field E_r. For a detector with responsitivity $\beta \approx S/P$, where P is the optical power incident on the detector, we choose E_r large enough so that $\beta |E_r|^2 \gg \delta S_{\mathrm{tech}}$, with δS_{tech} being the electronic noise in the closed-loop configuration.

[1] Genes, C., Vitali, D., Tombesi, P., Gigan, S., & Aspelmeyer, M. (2008). Ground-state cooling of a micromechanical oscillator: Comparing cold damping and cavity-assisted cooling schemes. Physical Review A, 77(3), 1-9. doi:10.1103/PhysRevA.77.033804